Report

Cell Reports

Smurf1 Inhibits Osteoblast Differentiation, Bone Formation, and Glucose Homeostasis through Serine 148

Graphical Abstract

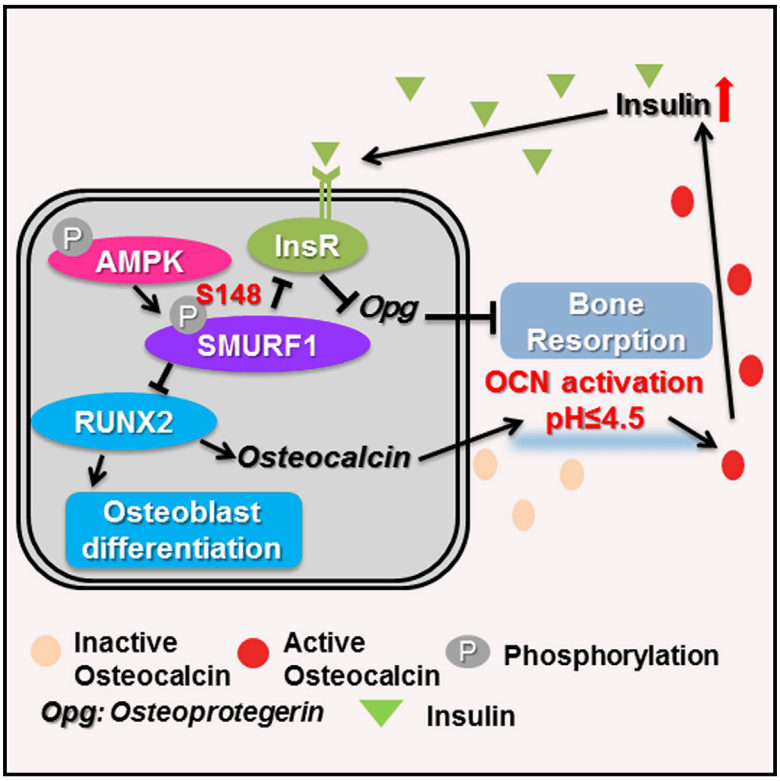

Authors

Junko Shimazu, Jianwen Wei, Gerard Karsenty

Correspondence

gk2172@columbia.edu

In Brief

Shimazu et al. identify Smurf1 as a determinant of osteoblast differentiation during the development of bone formation and glucose homeostasis post-natally by targeting Runx2 and InsR, respectively, for degradation in osteoblasts and demonstrates the necessity of serine 148 of Smurf1 for these functions.

Highlights

- Smurf1 inhibits osteoblast differentiation by targeting Runx2 for degradation
- This function of Smurf1 requires the presence of serine 148 (S148) in Smurf1
- S148 in Smurf1 in osteoblasts is also needed for targeting InsR for degradation
- Smurf1 regulates glucose metabolism by regulating InsR accumulation in osteoblasts

Shimazu et al., 2016, Cell Reports *15*, 27–35
April 5, 2016
http://dx.doi.org/10.1016/j.celrep.2016.03.003

CellPress

Cell Reports
Report

Smurf1 Inhibits Osteoblast Differentiation, Bone Formation, and Glucose Homeostasis through Serine 148

Junko Shimazu,[1] Jianwen Wei,[1] and Gerard Karsenty[1,*]
[1]Department of Genetics & Development, College of Physicians and Surgeons, Columbia University, New York, NY 10032, USA
*Correspondence: gk2172@columbia.edu
http://dx.doi.org/10.1016/j.celrep.2016.03.003

SUMMARY

The E3 ubiquitin ligase Smurf1 targets the master regulator of osteoblast differentiation, Runx2, for degradation, yet the function of Smurf1, if any, during osteoblast differentiation in vivo is ill defined. Here, we show that Smurf1 prevents osteoblast differentiation by decreasing Runx2 accumulation in osteoblasts. Remarkably, mice harboring a substitution mutation at serine 148 (S148) in Smurf1 that prevents its phosphorylation by AMPK (*Smurf1*$^{ki/ki}$) display a premature osteoblast differentiation phenotype that is equally severe as that of *Smurf1*$^{-/-}$ mice, as well as a high bone mass, and are also hyperinsulinemic and hypoglycemic. Consistent with the fact that Smurf1 targets the insulin receptor for degradation, there is, in *Smurf1*$^{ki/ki}$ mice, an increase in insulin signaling in osteoblasts that triggers a rise in the circulating levels of osteocalcin, a hormone that favors insulin secretion. These results identify Smurf1 as a determinant of osteoblast differentiation during the development of bone formation and glucose homeostasis post-natally and demonstrate the necessity of S148 for these functions.

INTRODUCTION

The transcription factor Runx2 has many attributes of a master regulator of osteoblast differentiation. In its absence, there are no osteoblasts anywhere in the skeleton, and its haploinsufficiency, by delaying osteoblast differentiation in bone formation through intramembranous ossification, results in a cleidocranial dysplasia (CCD), a disease characterized by open fontanelles and short clavicles (Ducy et al., 1997; Komori et al., 1997; Lee et al., 1997; Mundlos et al., 1997; Otto et al., 1997). Conversely, an increase in Runx2 activity, as seen in mice and humans lacking one allele of *Twist*, results in craniosynostosis because of a premature osteoblast differentiation in the skull, leading to early closure of the sutures (Bialek et al., 2004).

Not surprisingly, given the paramount importance of this transcription factor for skeletogenesis, the mechanisms regulating the accumulation of Runx2 in cells of the osteoblast lineage have been intensively studied. Runx2 accumulation in osteoblast progenitor cells and differentiated osteoblasts is regulated in part by ubiquitination, and several E3 ubiquitin ligases have been implicated in targeting Runx2 for degradation (Jones et al., 2006; Kaneki et al., 2006; Zhao et al., 2003). One of them Smurf1, interacts with Runx2 and other proteins regulating bone mass accrual such as Smad1, Smad5, MEKK2, and the insulin receptor (InsR) (Wei et al., 2014; Yamashita et al., 2005; Zhu et al., 1999). Consistent with these biochemical findings, forced expression of *Smurf1* in osteoblasts inhibits, whereas deletion of *Smurf1* in all cells favors, bone formation in adult mice (Yamashita et al., 2005; Zhao et al., 2004). It has been proposed that Smurf1 achieves these functions in part by targeting MEKK2 for degradation (Yamashita et al., 2005). Surprisingly, given the biochemical evidence indicating that Smurf1 favors the degradation of Runx2, no loss-of-function study has yet addressed the role of Smurf1 as a regulator of osteoblast differentiation in vivo.

A second important question regarding Smurf1 biology is to identify a domain, if not a single amino acid, that would confer to this protein the ability to target Runx2 for degradation in vivo. This question is even more relevant in view of the demonstration that, in vitro, Smurf1 must be phosphorylated by AMPK on serine 148 (S148) in order to trigger the degradation of Runx2 (Wei et al., 2015). This raises the question of the biological importance of this residue in the functions of Smurf1.

We have addressed the aforementioned questions by analyzing *Smurf1*$^{-/-}$ mice and mice harboring a mutated form of *Smurf1* in which S148 is mutated to alanine (*Smurf1*$^{ki/ki}$). We show here that *Smurf1* inhibits osteoblast differentiation through its ability to target Runx2 for degradation and that this function requires the presence of S148. Remarkably, *Smurf1*$^{ki/ki}$ mice are also hypoglycemic and hyperinsulinemic, because S148 is needed for Smurf1 ability to target the InsR for degradation. As a result, there is an accumulation of the InsR in the bones of *Smurf1*$^{ki/ki}$ mice. This leads to an increase in the circulating levels of the bioactive form of the bone-derived hormone osteocalcin that favors insulin secretion and can cause hypoglycemia (Ferron et al., 2010a; Lee et al., 2007). These results define critical functions of Smurf1 in cells of the osteoblast lineage throughout life and highlight the importance of S148 for Smurf1 ability to target Runx2 and InsR for degradation.

RESULTS

Smurf1 Regulates Osteoblast Differentiation

To determine whether *Smurf1* affects osteoblast differentiation in vivo, we analyzed, in post-natal day (P) 4 and P10 *Smurf1*$^{-/-}$ mice, two parameters that reflect the activity of Runx2 in cells of the osteoblast lineage during development: the closure of sutures in the skull and the length of clavicles.

Alcian blue/alizarin red staining of skeletal preparations showed that the clavicles of *Smurf1*$^{-/-}$ mice were significantly longer than those of wild-type (WT) mice (Figure 1A), and sagittal sutures of *Smurf1*$^{-/-}$ skulls showed evidence of craniosynostosis (Figures 1B and 1C). Next, we analyzed, by in situ hybridization, the expression of *Bone sialoprotein* (*Bsp*), a biomarker of osteoblast differentiation (Bialek et al., 2004) in the calvarial bones of embryonic day (E) 14.5 WT and *Smurf1*$^{-/-}$ embryos. The expression of *Bsp* was stronger in the calvarial bones of E14.5 *Smurf1*$^{-/-}$ than in those of WT embryos (Figure 1D). The same was true for the expression of *Bsp* and of *Osteocalcin* (*Ocn*), another osteoblast differentiation marker, in the femurs of E14.5 *Smurf1*$^{-/-}$ embryos, whether this was assayed by qPCR or by in situ hybridization (Figures 1E–1G). As a negative control in this experiment, we analyzed the expression of *α1(I) Collagen* (*α1(I)Col*), which is not regulated by Runx2 in vivo (Wei et al., 2015).

To link this premature osteoblast differentiation to an increase in Runx2 accumulation, we analyzed the abundance of this transcription factor in the skulls of *Smurf1*$^{-/-}$ and WT littermates and observed that Runx2 was more abundant in *Smurf1*$^{-/-}$ than in WT skulls (Figure 1H). This latter result explains the increase in the expression of *Ocn*, a target of Runx2 (Ducy et al., 1997) (Figures 1E, 1G, and 1I). Taken together, these results established that Smurf1 is a negative regulator of osteoblast differentiation in vivo and suggested that this function occurs, in part, by targeting Runx2 for degradation.

S148 Is Necessary for Smurf1 Ability to Inhibit Osteoblast Differentiation and Bone Formation

In vitro, the phosphorylation of Smurf1 by AMPK at S148 is needed for its ability to target Runx2 for degradation (Wei et al., 2015). Thus, we tested the importance of this residue for Smurf1 ability to inhibit osteoblast differentiation by analyzing mutant mice harboring a S148A mutation in *Smurf1* (*Smurf1*$^{ki/ki}$) (Figures S1A–S1C). A western blot analysis verified that the phosphorylation of Smurf1 at S148 was abolished in *Smurf1*$^{ki/ki}$ osteoblasts, although Smurf1 accumulation was not affected (Figure 2A).

Alcian blue/alizarin red staining of skeletal preparations showed that clavicles were significantly longer and sagittal sutures of the skulls were more closed in *Smurf1*$^{ki/ki}$ than in newborn WT mice (Figures 2B–2D). Accordingly, osteoblasts isolated from *Smurf1*$^{-/-}$ or *Smurf1*$^{ki/ki}$ mice formed more mineralized nodules than WT osteoblasts (Figure S2A). In vivo, *Bsp* expression was stronger in the calvarial bones of E14.5 *Smurf1*$^{ki/ki}$ embryos than in those of WT embryos (Figure 2E). The expression of *Ocn* started earlier, and the expression of *Bsp* was stronger in the femurs of *Smurf1*$^{ki/ki}$ than in those of E14.5 WT embryos, indicating that osteoblast differentiation occurred earlier in *Smurf1*$^{ki/ki}$ embryos throughout the skeleton. In contrast, no overt difference in the expression of *α1(I)Col* between E14.5 WT and *Smurf1*$^{ki/ki}$ embryos was noted (Figure 2F). The expression of *Ocn* and *Bsp* was also significantly higher in the femurs of E14.5 *Smurf1*$^{ki/ki}$ embryos than in those of WT embryos when measured by qPCR (Figures 2G and 2H).

That *Bsp* and *Ocn* expression was higher in the femurs of *Smurf1*$^{ki/ki}$ mice at P10 (Figures S2B and S2C) suggested that this S148A mutation in *Smurf1* may affect bone biology post-natally. Indeed, 2-month-old *Smurf1*$^{ki/ki}$ mice had a higher bone mass and higher trabecular number than WT littermates because of an increase in their osteoblast number and bone formation rate (Figures 2I–2L). These phenotypes could be traced, in part, to an increase in the accumulation of Runx2 in *Smurf1*$^{ki/ki}$ skulls (Figure 2M). To ascertain that the phosphorylation of Smurf1 at S148 is needed to target Runx2 for degradation, we performed a glutathione S-transferase (GST) pull-down assay and observed that the interaction between Smurf1 and Runx2 that occurred upon phosphorylation of Smurf1 by AMPK was abrogated when S148 was mutated to alanine. Accordingly, forced expression of WT, but not *S148A Smurf1*, decreased the accumulation of Runx2 in COS-7 cells (Figures 2N and 2O). Taken collectively, these data establish the importance of S148 for Smurf1 ability to inhibit osteoblast differentiation and bone formation.

Smurf1 Inhibits Osteoblast Differentiation by Targeting Runx2 to Degradation

If S148 is required for Smurf1 inhibition of osteoblast differentiation because it targets Runx2 for degradation, mutating S148 to alanine in Smurf1 should increase Runx2 accumulation and rescue, in part, the CCD phenotype seen in *Runx2*$^{+/-}$ mice (Komori et al., 1997; Otto et al., 1997). To test this hypothesis, we analyzed *Runx2*$^{+/-}$*;Smurf1*$^{ki/ki}$ mice.

Alcian blue/alizarin red staining of skeletal preparations showed a marked improvement of the CCD phenotype in *Runx2*$^{+/-}$*;Smurf1*$^{ki/ki}$, compared to that in *Runx2*$^{+/-}$ mice (Figures 3A–3C), while a western blot verified that Runx2 accumulation was increased in *Runx2*$^{+/-}$*;Smurf1*$^{ki/ki}$ skulls (Figure 3D). This increase in Runx2 accumulation resulted in an improved osteoblast differentiation, as shown by the increased *Ocn* expression in E15.5 *Runx2*$^{+/-}$*;Smurf1*$^{ki/ki}$ embryos, compared to *Runx2*$^{+/-}$ embryos (Figure 3E). Expression of *Ocn* and *Bsp* was also significantly higher in the bones of *Runx2*$^{+/-}$*;Smurf1*$^{ki/ki}$ mice, compared to those of *Runx2*$^{+/-}$ mice at P10 when measured by qPCR (Figures 3F and 3G).

Hence, the ability of Smurf1 to target Runx2 for degradation explains, to a large extent, why this E3 ubiquitin ligase inhibits osteoblast differentiation. That the rescue of the CCD phenotype was not complete in *Runx2*$^{+/-}$*;Smurf1*$^{ki/ki}$ mice is consistent with the notion that Smurf1 also acts through additional mechanisms to prevent osteoblast differentiation, such as targeting MEKK2, Smad1, and Smad5 for degradation (Yamashita et al., 2005; Zhu et al., 1999).

S148 Is Needed for Smurf1 Ability to Regulate Glucose Homeostasis

To determine whether S148 is necessary for the interaction of Smurf1 with its other substrates, we focused on the InsR,

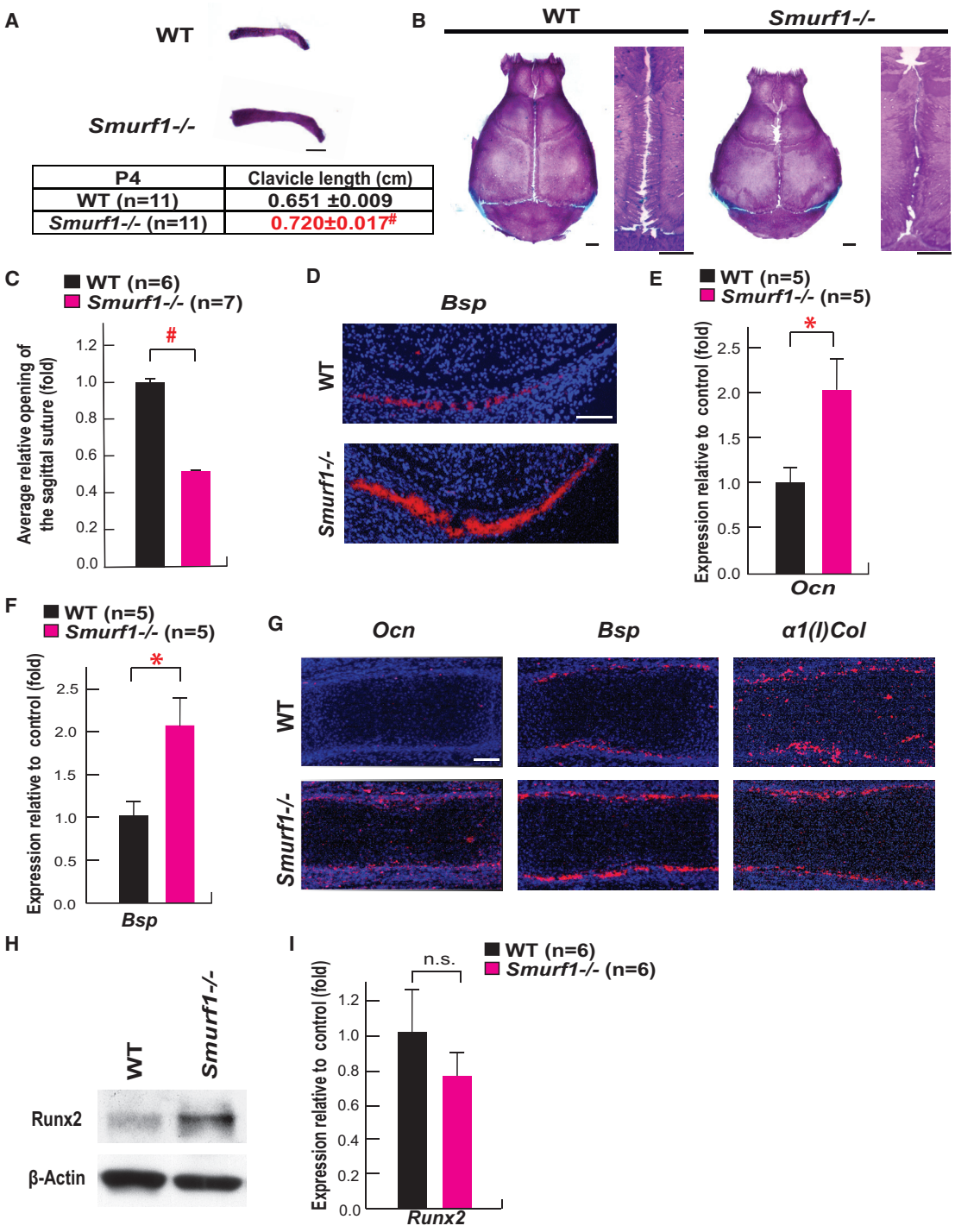

P4	Clavicle length (cm)
WT (n=11)	0.651 ±0.009
Smurf1-/- (n=11)	0.720±0.017#

Figure 1. Regulation of Osteoblast Differentiation by Smurf1 In Vivo

(A and B) Alcian blue/alizarin red staining of (A) clavicles and (B) skulls of P4 and P10 WT and *Smurf1*$^{-/-}$ mice, respectively. Scale bar, 1 mm.

(C) Opening of sagittal sutures in P10 *Smurf1*$^{-/-}$ and WT mice.

(D) In situ hybridization analysis of *Bsp* expression in calvarial bones of E14.5 *Smurf1*$^{-/-}$ and WT embryos. Scale bar, 100 μm.

(E and F) qPCR analysis of (E) *Ocn* and (F) *Bsp* expression in femurs of E14.5 WT and *Smurf1*$^{-/-}$ embryos (n = 5).

(G) In situ hybridization analysis of *Ocn*, *Bsp*, and *α1(I)Col* expression in femurs of E14.5 *Smurf1*$^{-/-}$ and WT embryos. Scale bar, 100 μm.

(H) Runx2 accumulation in skulls of P10 WT and *Smurf1*$^{-/-}$ mice.

(I) Expression of *Runx2* in the femurs of P10 WT and *Smurf1*$^{-/-}$ mice (n = 6). n.s., not significant.

Error bars indicate mean ± SEM. *p ≤ 0.05; #p ≤ 0.005 (compared to control), from Student's t tests.

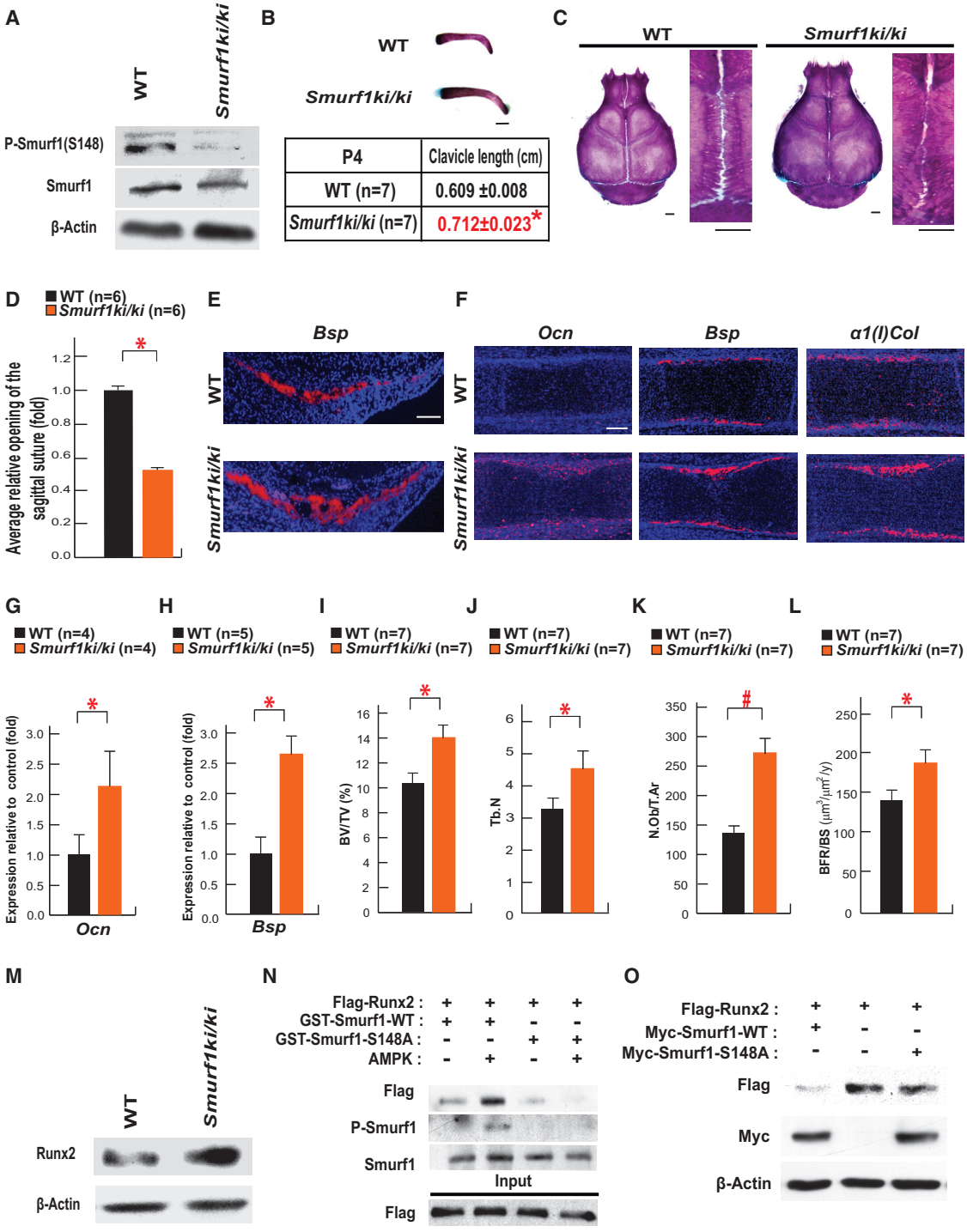

Figure 2. Phosphorylation of Smurf1 at S148 Is Necessary for Smurf1 Ability to Regulate Osteoblast Differentiation In Vivo

(A) Western blot analysis of S148 phosphorylation in Smurf1 in WT and *Smurf1*$^{ki/ki}$ osteoblasts.

(B and C) Alcian blue/alizarin red staining of (B) clavicles and (C) skulls of P4 and P10 WT and *Smurf1*$^{ki/ki}$ mice, respectively. Scale bar, 1 mm.

(D) Opening of sagittal sutures in P10 *Smurf1*$^{ki/ki}$ and WT mice.

(E and F) In situ hybridization analysis of (E) *Bsp* in calvarial bones and (F) *Ocn*, *Bsp*, and α*1(I)Col* expression in femurs of E14.5 WT and *Smurf1*$^{ki/ki}$ embryos. Scale bar, 100 μm.

(G and H) qPCR analysis of (G) *Ocn* and (H) *Bsp* expression in femurs of E14.5 WT and *Smurf1*$^{ki/ki}$ embryos (n = 4–5).

(legend continued on next page)

because both *Smurf1*$^{-/-}$ mice and *Smurf1*$^{ki/ki}$ mice were hypoglycemic and hyperinsulinemic (Figures 4A–4C).

Following its phosphorylation by AMPK, WT—but not S148A Smurf1—interacts readily with the InsR (Figure 4D), and forced expression of WT—but not *S148A Smurf1*—decreased the accumulation of InsR in COS-7 cells (Figure 4E). In vivo, the accumulation of the InsR was higher in *Smurf1*$^{-/-}$ and *Smurf1*$^{ki/ki}$ than in WT bones. That the accumulation of the InsR was not affected in other insulin target tissues, such as liver, white adipose tissue (WAT), and muscle in *Smurf1*$^{-/-}$ and *Smurf1*$^{ki/ki}$ mice (Figure 4F) is explained, in part, by the fact that *Smurf1* expression is markedly higher in bone than in the liver, WAT, and muscle (Figure 4G).

Given these observations, we tested whether the hypoglycemia seen in *Smurf1*$^{ki/ki}$ mice resulted, in part, from an increase in insulin signaling in osteoblasts. Since insulin signaling in osteoblasts inhibits *Osteoprotegerin* (*Opg*) expression (Ferron et al., 2010a), we used the expression of this gene in *Smurf1*$^{ki/ki}$ femurs as a readout of insulin signaling in osteoblasts. In agreement with the increased accumulation of the InsR in bone (Figure 4F), *Opg* expression was decreased in *Smurf1*$^{ki/ki}$ femurs compared to control femurs (Figure 4H), whereas *Rankl* expression was unchanged (Figure 4I). This decrease in *Opg* expression provides an explanation for the significant increase in the number of osteoclasts observed in the bones of adult *Smurf1*$^{ki/ki}$ mice (Figure 4J). This increase in bone resorption parameters was not of sufficient amplitude to compensate for the increase in bone formation parameters. As a result, *Smurf1*$^{ki/ki}$ mice had a high bone mass (Figures 2I–2L).

Since bone resorption is the mechanism whereby osteocalcin, a hormone that favors insulin secretion, is activated by decarboxylation (Ferron et al., 2010a), we measured the circulating levels of undercarboxyated and bioactive osteocalcin in control and *Smurf1*$^{ki/ki}$ mice and observed that circulating undercarboxylated osteocalcin levels were approximately 3-fold higher in *Smurf1*$^{ki/ki}$ mice than in control mice (Figure 4K). Such an increase in circulating osteocalcin levels should lead to a hyperinsulinemia and hypoglycemia as seen in *Smurf1*$^{ki/ki}$ mice (Figures 4B and 4C). To demonstrate that this increase in osteocalcin activity contributes to the hypoglycemia observed in *Smurf1*$^{ki/ki}$ mice, we analyzed *Smurf1*$^{ki/ki}$ mice lacking one allele of *Ocn* (*Smurf1*$^{ki/ki}$*;Ocn*$^{+/-}$). As shown in Figure 4L, blood glucose levels were normal in *Smurf1*$^{ki/ki}$*;Ocn*$^{+/-}$ mice. These results reveal the existence of a Smurf1-InsR-osteoprotegerin-osteocalcin pathway taking place in osteoblasts and contributing to glucose homeostasis.

DISCUSSION

The mechanisms regulating Runx2 accumulation in osteoblast progenitor cells have been a topic of intense investigation. This has led to the identification, mostly on biochemical grounds, of several E3 ubiquitin ligases that would trigger Runx2 for degradation. Given the number of E3 ubiquitin ligases known to interact with Runx2, one could fear that disrupting the interaction of only one of them with Runx2 would not significantly hamper osteoblast differentiation in vivo. Instead, our investigation shows that deleting a single E3 ubiquitin ligase implicated in Runx2 degradation *Smurf1* results in an increase in Runx2 accumulation, leading to a premature osteoblast differentiation during embryonic development and increased bone formation post-natally. Furthermore, we show that the majority of this function of Smurf1 requires a single amino acid, S148, to be phosphorylated by AMPK (Wei et al., 2015). These results highlight the importance of Smurf1 and of this particular residue in this molecule in targeting Runx2 for degradation in vivo and regulating osteoblast differentiation.

The functions of Smurf1 in osteoblasts extend beyond osteoblast differentiation and bone formation, since, by favoring the degradation of the InsR in osteoblasts, Smurf1 is a regulator of circulating osteocalcin levels. This explains the existence of hyperinsulinemia and hypoglycemia in *Smurf1*$^{ki/ki}$ mice. Indeed, Smurf1 regulates bone resorption and the production of the active form of osteocalcin, a hormone that favors insulin secretion (Lee et al., 2007). As it is the case for its ability to regulate osteoblast differentiation, this function of Smurf1 requires the presence of S148. Altogether, our results provide a deeper understanding of the molecular regulation of Runx2 accumulation and of the endocrine functions of bone.

EXPERIMENTAL PROCEDURES

Mice Generation

To generate *Smurf1*$^{Ki/+}$ mice, a mutation was introduced into a bacterial artificial chromosome (BAC) by recombineering, using the *galK* selection system (Warming et al., 2005). In the first step, the *galK* cassette was inserted into a BAC by homologous recombination, and clones were obtained through positive selection on minimal media plates on which galactose was the only carbon source. The successful recombination was validated by PCR analysis. In the second step, the *galK* cassette was substituted by double-stranded oligonucleotides, with the modified base pair in the middle of the homology arms flanking the *galK* casette. This step was achieved by negatively selecting against the *galK* cassette by resistance to 2-deoxy-galactose (DOG) on plates with glycerol as the carbon source. Clones in which the *galK* cassette is replaced by a mutation of interest were identified by PCR and sequencing. A *frt-neo-frt* (*FNF*) cassette was inserted upstream of the mutation and retrieved into the pMCS-DTA vector by homologous recombination using standard protocol. The targeting vector that was verified by PCR, diagnostic digestions, and sequencing was electroporated into embryonic stem (ES) cells, and positive ES cells were identified by PCR screening and sequencing. Selected ES cells were injected in 129Sv/EV blastocysts to generate chimeric mice. Chimeric mice were crossed to Gt(ROSA)26Sor$^{tm1(FLP1)Dym}$ to remove the neomycin-resistance cassette (Figures S1A–S1C).

Runx2$^{+/-}$ mice were generated previously (Otto et al., 1997). *Smurf1*$^{+/-}$ mice were a generous gift of Dr. Jeff Wrana (University of Toronto) (Narimatsu et al., 2009). All mice strains were maintained on a C57/129 mixed background,

(I–L) Bone histomorphometric analysis of L3 and L4 vertebrae of 2-month-old WT and *Smurf1*$^{ki/ki}$ female mice (n = 7). (I) Mineralized bone volume per total volume (BV/TV). (J) Trabecular number (Tb.N). (K) Osteoblast number per tissue area (N.Ob/T.Ar). (L) The annual fractional volume of trabecular bone formed per unit trabecular surface area (BFR/BS).

(M) Runx2 accumulation in the skulls of P10 WT and *Smurf1*$^{ki/ki}$ mice.

(N) GST pull-down assay showing interaction of Flag-Runx2 with GST-Smurf1 WT or S148A after phosphorylation by AMPK.

(O) Effect of the forced expression of WT or *S148A Smurf1* on the accumulation of Runx2 in COS-7 cells.

Error bars indicate mean ± SEM. *p $\leq$ 0.05; #p $\leq$ 0.005 (compared to control), from Student's t tests.

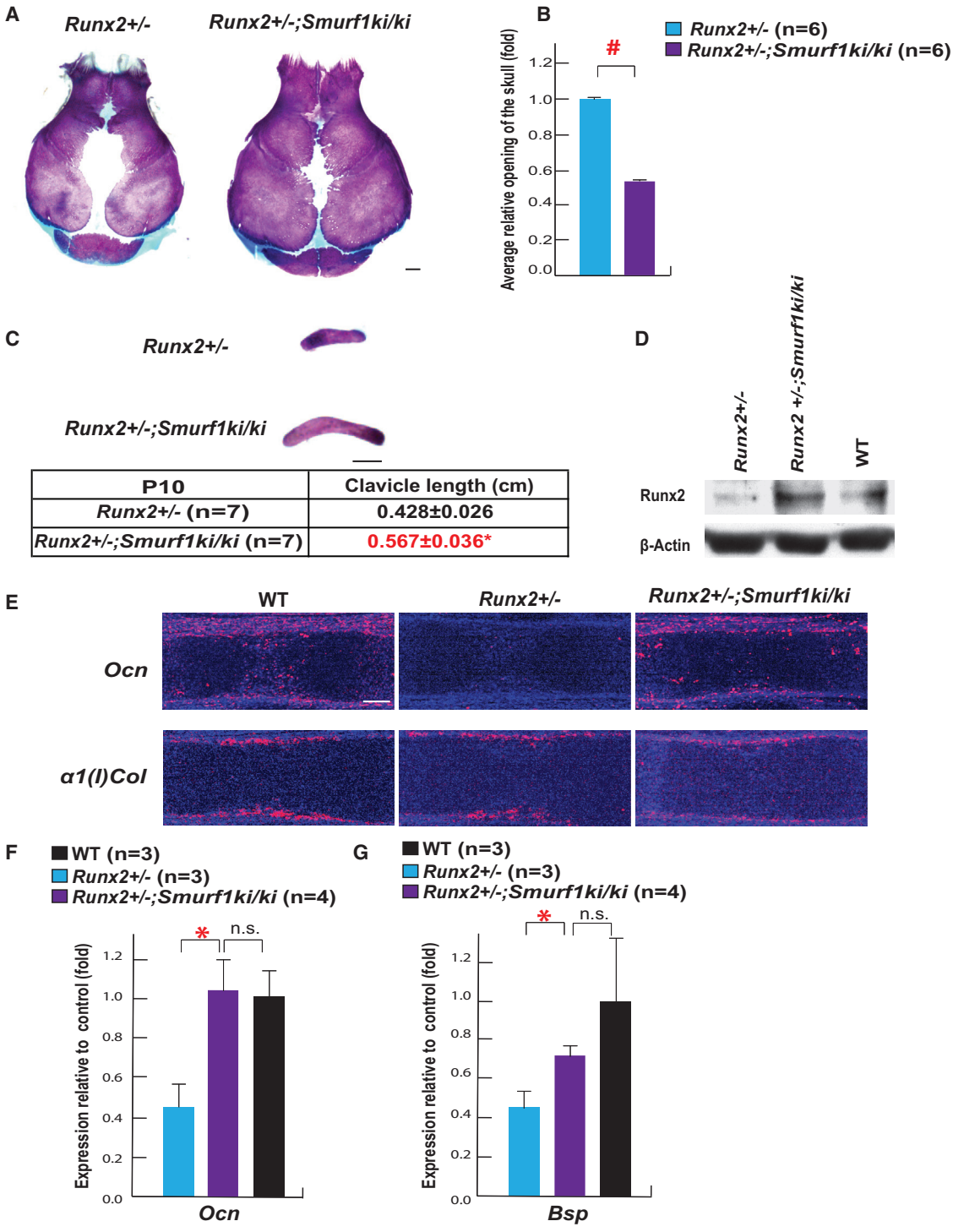

P10	Clavicle length (cm)
Runx2+/- (n=7)	0.428±0.026
Runx2+/-;Smurf1ki/ki (n=7)	0.567±0.036*

Figure 3. Smurf1 Phosphorylation at S148 Is Necessary to Regulate RUNX2 In Vivo

(A) Alcian blue/alizarin red staining of skulls of P10 *Runx2*$^{+/-}$ and *Runx2*$^{+/-}$;*Smurf1*$^{ki/ki}$ mice. Scale bar, 1 mm.

(B) Area of the opening of skulls in P10 *Runx2*$^{+/-}$;*Smurf1*$^{ki/ki}$ and *Runx2*$^{+/-}$ mice.

(C) Alcian blue/alizarin red staining of clavicles of P10 *Runx2*$^{+/-}$ and *Runx2*$^{+/-}$;*Smurf1*$^{ki/ki}$ mice. Scale bar, 1 mm.

(D) Runx2 accumulation in skulls of P10 *Runx2*$^{+/-}$, *Runx2*$^{+/-}$;*Smurf1*$^{ki/ki}$, and WT skulls.

(E) In situ hybridization analysis of *Ocn* and *α1(I)Col* expression in E15.5 WT, *Runx2*$^{+/-}$, and *Runx2*$^{+/-}$;*Smurf1*$^{ki/ki}$ femurs. Scale bar, 100 μm.

(F and G) qPCR analysis of (F) *Ocn* and (G) *Bsp* expression in femurs of P10 WT, *Runx2*$^{+/-}$, and *Runx2*$^{+/-}$;*Smurf1*$^{ki/ki}$ mice (n = 3–4).

Error bars indicate mean ± SEM. *p ≤ 0.05; #p ≤ 0.005 (compared to control), from Student's t tests.

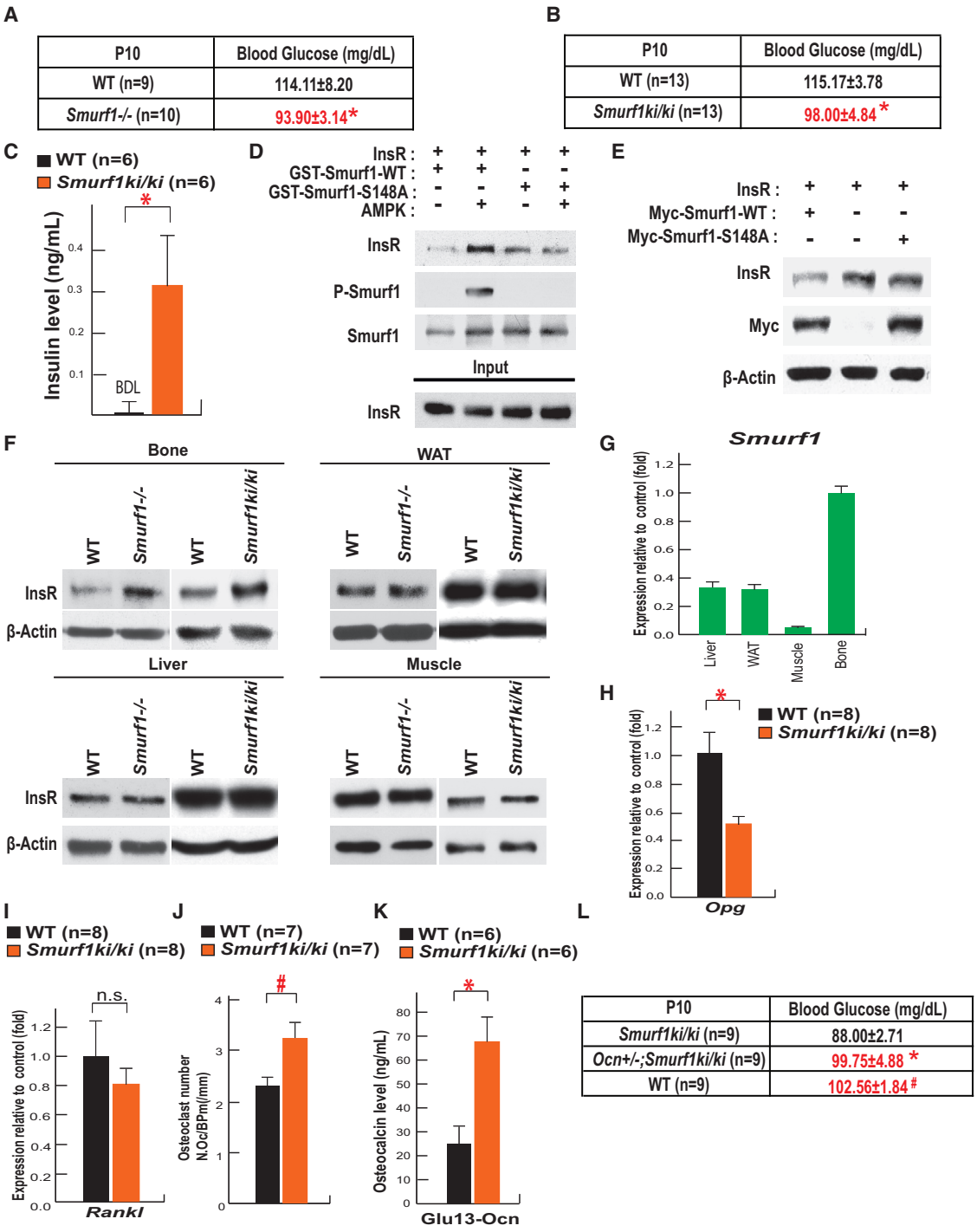

Figure 4. Phosphorylation of SMURF1 at S148 Is Necessary for Smurf1 Activity to Regulate InsR Degradation

(A and B) Blood glucose levels in (A) P10 WT and *Smurf1*$^{-/-}$ mice and (B) P10 WT and *Smurf1*$^{ki/ki}$ mice (n = 9–13 per group).

(C) Circulating insulin levels in P10 WT and *Smurf1*$^{ki/ki}$ mice (n = 6). BDL, below detection limit.

(D) GST pull-down assay showing interaction of InsR with GST-Smurf1 WT or GST-Smurf1 S148A after AMPK phosphorylation.

(E) Effect of the overexpression of WT or *S148A Smurf1* on the accumulation of InsR in COS-7 cells.

(F) Accumulation of the InsR in skull, liver, WAT, and muscle of P10 WT, *Smurf1*$^{-/-}$, and *Smurf1*$^{ki/ki}$ mice.

(G) Expression of *Smurf1* in liver, WAT, muscle, and skull of P10 WT mice.

(H and I) Expression of (H) *Opg* and (I) *Rankl* in the femurs of P10 WT and *Smurf1*$^{ki/ki}$ mice (n = 8). n.s., not significant.

(legend continued on next page)

except for *Runx2*$^{+/-}$ mice, which were maintained on a C57 background. Littermates were used as controls in all experiments. All procedures involving animals were approved by CUMC IACUC and conform to the relevant regulatory standards.

Cell Culture

Primary mouse calvaria osteoblasts were cultured as described previously (Ducy and Karsenty, 1995). To determine the formation of mineralized nodules, von Kossa staining was performed on osteoblasts cultured in differentiation medium supplemented with 5 mM β-glycerophosphate and 100 μg/ml ascorbic acid for 7 days. To detect the S148 phosphorylation in Smurf1, osteoblasts isolated from *Smurf1*$^{ki/ki}$ and WT pups were incubated overnight in glucose-free KRH buffer (50 mM HEPES, pH 7.4, 136 mM NaCl, 4.7 mM KCl, 1.25 mM $MgSO_4$, 1.25mM $CaCl_2$, and 0.1% BSA) and followed by western blot analysis.

DNA Transfection Experiments

Myc-Smurf1 WT and *S148A* plasmids were constructed by inserting a full-length cDNA of mouse *Smurf1* WT or *S148A* into pcDNA 3.1/myc-His B vector (Invitrogen). *Myc-Smurf1* WT or *S148A* was co-transfected with *Flag-Runx2* or the human *InsR* cDNA expression constructs (Wei et al., 2014, 2015) in COS-7 cells. DNA transfection experiments were performed using Lipofectamin 2000 (Invitrogen), according to the manufacturer's protocol.

Western Blot Analysis

Anti-Runx2 antibody (Santa Cruz Biotechnology), anti-β-Actin (Sigma), Anti-Smurf1, and Anti-Phospho-Ser148 Smurf1 (GenScript) were used. Other antibodies were obtained from Cell Signaling Technology. All western blot analyses were repeated at least three times, with different samples.

Gene Expression Analysis

RNA samples were extracted using TRIzol reagent (Invitrogen). Using 2 μg total RNA, cDNA preparation was carried out following standard protocols. The cDNAs were used as templates for qPCR analyses using CFX-Connect Real-Time PCR Detection System (Bio-Rad). Expression levels of each gene analyzed by qPCR were normalized using GAPDH (glyceraldehyde-3-phosphate dehydrogenase) expression levels as an internal control. The sequences of specific primers used in this study were previously described (Obri et al., 2014).

Skeletal Preparation and Analysis

Alcian blue/alizarin red staining of the skeletal preparation was conducted according to standard protocols (McLeod, 1980). Littermate controls were analyzed in all experiments. Quantifications of the length of clavicles, as well as the area of the opening of the skull, were made using ImageJ.

Bone Histomorphometry

This analysis was performed on L3 and L4 vertebrae of 2-month-old female mice as described previously (Chappard et al., 1987; Parfitt et al., 1987). Mineralized bone volume over the total tissue volume, osteoblast number per tissue area as well as trabecular number, and bone formation rate per bone surface were measured by conducting Von Kossa/van Gieson staining, toluidine blue staining, and calcein double labeling, respectively. Osteoclast parameters were measured by TRAP staining, followed by counterstain with hematoxylin. Osteoclasts were defined as multinucleated dark red cells along the bone surface. Histomorphometric analysis was performed using the OsteoMeasure System (OsteoMetrics).

Biochemistry

ELISAs were performed according to the manufacturer's instructions to measure mouse insulin (EZRMI-13K, Millipore) and undercarboxylated osteocalcin (Ferron et al., 2010b). For the AMPK phosphorylation assay, GST-Smurf1 and GST-Runx2 constructs were generated and purified as previously described (Ferron et al., 2013; Wei et al., 2015). The AMPK phosphorylation assay of GST-Smurf1 WT and S148A was performed using a previously described method (Wei et al., 2015).

GST Pull-Down Assay

GST-Smurf1 WT and GST-Smurf1 S148A were bound to glutathione agarose beads (GE Healthcare) and blocked overnight at 4°C in 5% BSA with end-over-end mixing. Beads were washed with AMPK assay buffer five times, and the AMPK phosphorylation assay was followed. Beads were washed with binding buffer (50 mM Tris-HCl, pH 7.5, 100 mM NaCl, 50 mM β-glycerophosphate, 10% glycerol, 1% Tween-20, 1 mM EDTA, 25 mM NaF) five times. Cell lysates of transfected COS-7 cells were incubated with 25 μg of GST for 2 hr at 4°C with end-over-end mixing. This mixture was centrifuged, and supernatants were mixed with GST-Smurf1 WT or S148A in 500 μl of binding buffer for 2 hr at 4°C with end-over-end mixing. The mixtures were washed five times and analyzed by SDS-PAGE followed by immunoblotting.

In Situ Hybridization

Tissues were fixed in 4% paraformaldehyde/PBS overnight at 4°C and then embedded in paraffin after serial dehydrations. Tissues were sectioned at 5 μm. In situ hybridization was performed using ^{35}S-labeled riboprobe as described previously (Ducy et al., 1997). The *α1(I)Col*, *Bsp*, and *Ocn* probes were prepared as previously described (Takeda et al., 2001). Hybridizations were performed overnight at 55°C, and washes were performed at 63°C. Autoradiography was performed as previously described (Sundin et al., 1990), and nuclei were counterstained with DAPI.

Statistics

All data are presented as mean ± SEM. In this paper, statistical analysis was performed by unpaired Student's t test. * denotes $p \leq 0.05$, and # denotes $p \leq 0.005$ compared to control.

SUPPLEMENTAL INFORMATION

Supplemental Information includes two figures and can be found with this article online at http://dx.doi.org/10.1016/j.celrep.2016.03.003.

AUTHOR CONTRIBUTIONS

Conceptualization, G.K., J.S., and J.W.; Methodology, J.S.; Investigation, J.S. and J.W.; Writing – Original Draft, G.K. and J.S.; Writing – Review & Editing, G.K., J.S., and J.W.; Funding Acquisition, G.K. and J.S.; Supervision, G.K.

ACKNOWLEDGMENTS

We thank Dr. C.-S. Lin and F. Lee for generation of *Smurf1 S148A* knockin mice, and we thank Drs. P. Ducy and J. Wrana for critical reading of the manuscript and for providing the *Smurf1*$^{+/-}$ mice, respectively. This work is supported by grants RO1DK104727-A1 and PO1AG032959-06A1 (G.K.), a Honjo International Scholarship (J.S.), and a Mandl fellowship (J.W.). The training program in Genetics and Development (J.S.) is supported by an NIH T32 training grant from the National Institute of General Medical Science.

Received: October 26, 2015
Revised: January 30, 2016
Accepted: February 25, 2016
Published: March 24, 2016

(J) Osteoclast number (N.Oc)/bone perimeter (B.Pm) (/mm) in 2-month-old WT and *Smurf1*$^{ki/ki}$ female mice (n = 7).
(K) Serum levels of undercarboxylated osteocalcin in 2-month-old WT and *Smurf1*$^{ki/ki}$ mice (n = 6).
(L) Blood glucose levels in P10 WT, *Smurf1*$^{ki/ki}$, and *Ocn*$^{+/-}$;*Smurf1*$^{ki/ki}$ mice (n = 9).
Error bars indicate mean ± SEM. *$p \leq 0.05$; #$p \leq 0.005$ (compared to control), from Student's t tests.

REFERENCES

Bialek, P., Kern, B., Yang, X., Schrock, M., Sosic, D., Hong, N., Wu, H., Yu, K., Ornitz, D.M., Olson, E.N., et al. (2004). A twist code determines the onset of osteoblast differentiation. Dev. Cell *6*, 423–435.

Chappard, D., Palle, S., Alexandre, C., Vico, L., and Riffat, G. (1987). Bone embedding in pure methyl methacrylate at low temperature preserves enzyme activities. Acta Histochem. *81*, 183–190.

Ducy, P., and Karsenty, G. (1995). Two distinct osteoblast-specific cis-acting elements control expression of a mouse osteocalcin gene. Mol. Cell. Biol. *15*, 1858–1869.

Ducy, P., Zhang, R., Geoffroy, V., Ridall, A.L., and Karsenty, G. (1997). Osf2/Cbfa1: a transcriptional activator of osteoblast differentiation. Cell *89*, 747–754.

Ferron, M., Wei, J., Yoshizawa, T., Del Fattore, A., DePinho, R.A., Teti, A., Ducy, P., and Karsenty, G. (2010a). Insulin signaling in osteoblasts integrates bone remodeling and energy metabolism. Cell *142*, 296–308.

Ferron, M., Wei, J., Yoshizawa, T., Ducy, P., and Karsenty, G. (2010b). An ELISA-based method to quantify osteocalcin carboxylation in mice. Biochem. Biophys. Res. Commun. *397*, 691–696.

Ferron, M., Settembre, C., Shimazu, J., Lacombe, J., Kato, S., Rawlings, D.J., Ballabio, A., and Karsenty, G. (2013). A RANKL-PKCβ-TFEB signaling cascade is necessary for lysosomal biogenesis in osteoclasts. Genes Dev. *27*, 955–969.

Jones, D.C., Wein, M.N., Oukka, M., Hofstaetter, J.G., Glimcher, M.J., and Glimcher, L.H. (2006). Regulation of adult bone mass by the zinc finger adapter protein Schnurri-3. Science *312*, 1223–1227.

Kaneki, H., Guo, R., Chen, D., Yao, Z., Schwarz, E.M., Zhang, Y.E., Boyce, B.F., and Xing, L. (2006). Tumor necrosis factor promotes Runx2 degradation through up-regulation of Smurf1 and Smurf2 in osteoblasts. J. Biol. Chem. *281*, 4326–4333.

Komori, T., Yagi, H., Nomura, S., Yamaguchi, A., Sasaki, K., Deguchi, K., Shimizu, Y., Bronson, R.T., Gao, Y.H., Inada, M., et al. (1997). Targeted disruption of Cbfa1 results in a complete lack of bone formation owing to maturational arrest of osteoblasts. Cell *89*, 755–764.

Lee, B., Thirunavukkarasu, K., Zhou, L., Pastore, L., Baldini, A., Hecht, J., Geoffroy, V., Ducy, P., and Karsenty, G. (1997). Missense mutations abolishing DNA binding of the osteoblast-specific transcription factor OSF2/CBFA1 in cleidocranial dysplasia. Nat. Genet. *16*, 307–310.

Lee, N.K., Sowa, H., Hinoi, E., Ferron, M., Ahn, J.D., Confavreux, C., Dacquin, R., Mee, P.J., McKee, M.D., Jung, D.Y., et al. (2007). Endocrine regulation of energy metabolism by the skeleton. Cell *130*, 456–469.

McLeod, M.J. (1980). Differential staining of cartilage and bone in whole mouse fetuses by alcian blue and alizarin red S. Teratology *22*, 299–301.

Mundlos, S., Otto, F., Mundlos, C., Mulliken, J.B., Aylsworth, A.S., Albright, S., Lindhout, D., Cole, W.G., Henn, W., Knoll, J.H., et al. (1997). Mutations involving the transcription factor CBFA1 cause cleidocranial dysplasia. Cell *89*, 773–779.

Narimatsu, M., Bose, R., Pye, M., Zhang, L., Miller, B., Ching, P., Sakuma, R., Luga, V., Roncari, L., Attisano, L., and Wrana, J.L. (2009). Regulation of planar cell polarity by Smurf ubiquitin ligases. Cell *137*, 295–307.

Obri, A., Makinistoglu, M.P., Zhang, H., and Karsenty, G. (2014). HDAC4 integrates PTH and sympathetic signaling in osteoblasts. J. Cell Biol. *205*, 771–780.

Otto, F., Thornell, A.P., Crompton, T., Denzel, A., Gilmour, K.C., Rosewell, I.R., Stamp, G.W., Beddington, R.S., Mundlos, S., Olsen, B.R., et al. (1997). Cbfa1, a candidate gene for cleidocranial dysplasia syndrome, is essential for osteoblast differentiation and bone development. Cell *89*, 765–771.

Parfitt, A.M., Drezner, M.K., Glorieux, F.H., Kanis, J.A., Malluche, H., Meunier, P.J., Ott, S.M., and Recker, R.R. (1987). Bone histomorphometry: standardization of nomenclature, symbols, and units. Report of the ASBMR Histomorphometry Nomenclature Committee. J. Bone Miner. Res. *2*, 595–610.

Sundin, O.H., Busse, H.G., Rogers, M.B., Gudas, L.J., and Eichele, G. (1990). Region-specific expression in early chick and mouse embryos of Ghox-lab and Hox 1.6, vertebrate homeobox-containing genes related to Drosophila labial. Development *108*, 47–58.

Takeda, S., Bonnamy, J.P., Owen, M.J., Ducy, P., and Karsenty, G. (2001). Continuous expression of Cbfa1 in nonhypertrophic chondrocytes uncovers its ability to induce hypertrophic chondrocyte differentiation and partially rescues Cbfa1-deficient mice. Genes Dev. *15*, 467–481.

Warming, S., Costantino, N., Court, D.L., Jenkins, N.A., and Copeland, N.G. (2005). Simple and highly efficient BAC recombineering using galK selection. Nucleic Acids Res. *33*, e36.

Wei, J., Ferron, M., Clarke, C.J., Hannun, Y.A., Jiang, H., Blaner, W.S., and Karsenty, G. (2014). Bone-specific insulin resistance disrupts whole-body glucose homeostasis via decreased osteocalcin activation. J. Clin. Invest. *124*, 1–13.

Wei, J., Shimazu, J., Makinistoglu, M.P., Maurizi, A., Kajimura, D., Zong, H., Takarada, T., Iezaki, T., Pessin, J.E., Hinoi, E., and Karsenty, G. (2015). Glucose uptake and Runx2 synergize to orchestrate osteoblast differentiation and bone formation. Cell *161*, 1576–1591.

Yamashita, M., Ying, S.X., Zhang, G.M., Li, C., Cheng, S.Y., Deng, C.X., and Zhang, Y.E. (2005). Ubiquitin ligase Smurf1 controls osteoblast activity and bone homeostasis by targeting MEKK2 for degradation. Cell *121*, 101–113.

Zhao, M., Qiao, M., Oyajobi, B.O., Mundy, G.R., and Chen, D. (2003). E3 ubiquitin ligase Smurf1 mediates core-binding factor alpha1/Runx2 degradation and plays a specific role in osteoblast differentiation. J. Biol. Chem. *278*, 27939–27944.

Zhao, M., Qiao, M., Harris, S.E., Oyajobi, B.O., Mundy, G.R., and Chen, D. (2004). Smurf1 inhibits osteoblast differentiation and bone formation in vitro and in vivo. J. Biol. Chem. *279*, 12854–12859.

Zhu, H., Kavsak, P., Abdollah, S., Wrana, J.L., and Thomsen, G.H. (1999). A SMAD ubiquitin ligase targets the BMP pathway and affects embryonic pattern formation. Nature *400*, 687–693.